Biosensors and Bioelectronics 126 (2019) 315–323

Contents lists available at ScienceDirect

Biosensors and Bioelectronics

journal homepage: www.elsevier.com/locate/bios

Disk-based one-dimensional photonic crystal slabs for label-free immunosensing

Gabriel Sancho-Fornes[a], Miquel Avella-Oliver[a], Javier Carrascosa[a], Estrella Fernandez[a], Eva M. Brun[a], Ángel Maquieira[a,b,*]

[a] Instituto Interuniversitario de Investigación de Reconocimiento Molecular y Desarrollo Tecnológico (IDM), Universitat Politècnica de València, Universitat de València, Camino de Vera s/n, 46022 Valencia, Spain
[b] Departamento de Química, Universitat Politècnica de València, Camino de Vera s/n, 46022 Valencia, Spain

ARTICLE INFO

Keywords:
Photonic crystal
Guided-mode resonance
Diffraction
Blu-ray
Immunosensing
Label-free

ABSTRACT

One-dimensional photonic crystal slabs are periodic optical nanostructures that produce guided-mode resonance. They couple part of the incident light into the waveguide generating bandgaps in the transmittance spectrum, whose position is sensitive to refractive index variations on their surface. In this study, we present one-dimensional photonic crystal slab biosensors based on the internal nanogrooved structure of Blu-ray disks for label-free immunosensing. We demonstrated that this polycarbonate structure coated with a critical thickness of TiO_2 generates guided-mode resonance. Its optical behavior was established comparing it with other compact disk structures. The results were theoretically calculated and experimentally demonstrated, all them being in agreement. The bioanalytical performance of these photonic crystals was experimentally demonstrated in a model assay to quantify IgGs as well as in two immunoassays to determine the biomarkers C-reactive protein and lactate dehydrogenase (detection limits of 0.1, 87, and 13 nM, respectively). The results are promising towards the development of new low-cost, portable, and label-free optical biosensors that join these photonic crystals with dedicated bioanalytical scanners based on compact disk drives.

1. Introduction

There is an increasing social demand of point-of-care analytical systems (Li et al., 2017; Ranjan et al., 2017; St John and Price, 2014), which highlights the need of scientific advances that supports the development of biosensors towards the ASSURED criteria outlined by the World Health Organization (Kettler et al., 2004). The design of biosensors capable of analyzing unlabeled biointeractions provide appealing solutions in this direction, mainly in terms of simplicity and reliability (Carrascosa et al., 2016; Citartan et al., 2013; Fathi et al., 2018; Zanchetta et al., 2017). On the other hand, the impact of these systems on the point-of-care scenario is strongly restricted by the low scalability, high complexity, and costs of the materials and nanofabrication methods on which the state-of-the-art label-free biosensing approaches are based (Nikov et al., 2017; Yamada et al., 2017).

Photonic crystals (PCs) are a popular class of optical biosensing materials that enable label-free analysis format (Zhang et al., 2015). They are nanostructured systems constituted by alternated materials with different refractive indexes that extend along one, two, or three directions in a periodic fashion (Inan et al., 2017). PCs interact with light generating higher (bands) and lower (bandgaps) intensity regions in the reflected and transmitted spectra (Fenzl et al., 2014; Joannopoulos et al., 2008). These materials are typically used as refractometric biosensors to sense unlabeled biointeractions, where they are tailored to modify their light filtering properties upon refractive index variations (on or into the material) and used as substrates for heterogeneous biorecognition assays. This strategy has been employed for several biosensing purposes, such as analyzing binding affinities (Zlatanovic et al., 2009) and quantifying biointeractions in fields as chemical analysis, drug screening, biomedical detection, environmental monitoring, and food safety (Konopsky and Alieva, 2007; Lin et al., 2017; Michael et al., 2016; Yan et al., 2017).

Linear photonic crystal slabs exploit guided-mode resonance (GMR) for light filtering and present interesting features for biosensing (Hermannsson et al., 2015; Inan et al., 2017; Karrock et al., 2017; Threm et al., 2012). These systems are constituted by one-dimensional surface relief gratings, coated with a thin film of a high refractive index material, such as TiO_2 or Ta_2O_5, acting as a waveguide. They use light

* Corresponding author at: Instituto Interuniversitario de Investigación de Reconocimiento Molecular y Desarrollo Tecnológico (IDM), Universitat Politècnica de València, Universitat de València, Camino de Vera s/n, 46022 Valencia, Spain.
E-mail address: amaquieira@qim.upv.es (Á. Maquieira).

https://doi.org/10.1016/j.bios.2018.11.005
Received 25 October 2018; Accepted 2 November 2018
Available online 03 November 2018
0956-5663/

coupling mediated by diffractive gratings into a guided mode which propagates through the deposited TiO_2 but it slowly leaks out from the TiO_2 layer. The leaked wave interferes with the applied wave to produce a filter response and generate sharp bandgaps in the transmission spectra (Lin and Huang, 2016). Changes in the refractive index on these materials cause wavelength shifts in the filtered light. This phenomenon can be exploited to sense biorecognition assays on the surface of these photonic crystals (Nazirizadeh et al., 2010). Promising advances have been reached in this direction for the development of immunoassays and DNA hybridization analysis (Su et al., 2018; Wang et al., 2018) on GMR structures obtained by standard nanofabrication techniques, typically nanolithography and e-beam (Shafiee et al., 2014; Sørensen et al., 2018).

Exploiting the resources of the consumer electronics is a smart way to address the development of biosensors (Avella-Oliver et al., 2016; Vashist et al., 2015). Among the different mass-produced technologies, compact disk systems entail a particular high potential for this purpose, as demonstrated in many approaches for sensing labelled biorecognition assays (Morais et al., 2016)(Yu et al., 2013). As well as -shown in a few recent studies- for label-free biosensing by means of surface-enhanced Raman scattering (Avella-Oliver et al., 2017b), Fano resonance (López-Muñoz et al., 2017), and diffraction-based sensing (Avella-Oliver et al., 2017a).

Herein we introduce a simple and cost-effective PC slab (1-D) based on the internal structure of the disks (see Fig. S1 and Table S1) coated with a high refractive index dielectric material (TiO_2) as a new platform for label-free biosensing. The detection system consisted of a white light source and a fiber-coupled spectrometer that collects the transmitted light. The internal structure of the compact disks performs as diffraction grating, diffracting an external wave, and coupling it into a guided mode that propagates through the deposited TiO_2, as illustrated in Fig. 1B. The TiO_2 layer shows an excellent adherence to the polycarbonate substrate and also provides a suitable surface where to attach probes in a covalent way through the organosilane chemistry. First, this study reports the fabrication of these photonic crystals, explores their response with the most widespread compact disk technologies (CD, DVD, and Blu-ray) and different TiO_2 thicknesses, and determines the optimal configuration considering experimental results and simulations. Then, we characterize the structural and optical features of these nanomaterials, develop a suitable detection system, and experimentally prove the concept using a model immunoassay system to determine immunoglobulins. Finally, we employed these substrates to quantify disease biomarkers such as C-reactive protein and lactate dehydrogenase.

2. Experimental section

2.1. Materials

Phosphate buffered saline (PBS, 8 mM Na_2HPO_4, 2 mM KH_2PO_4, 137 mM NaCl, 2.7 mM KCl, pH 7.4) and PBS-T (PBS with 0.05% v/v Tween 20, pH 7.4) were prepared with purified water (Milli-Q, Millipore Iberica, Madrid, Spain) and filtered through a 0.2 μm pore size membranes (Fisher Scientific, Madrid, Spain) before use. Glutaraldehyde solution (25 wt% in H_2O), (3-Aminopropyl)triethoxysilane (99%), bovine serum albumin (BSA), lactate dehydrogenase from rabbit muscle (LDH), C-reactive protein (CRP), mouse anti-CRP, rabbit anti-BSA, goat IgG, rabbit IgG and goat anti-rabbit were purchased from Sigma Aldrich (Madrid, Spain). Rabbit anti-LDH was obtained by rabbit immunization. Mouse IgG was kindly provided by Igenasa S.A. (Madrid, Spain). Sucrose was provided by Scharlau Chemie (Barcelona, Spain). Standard recordable compact disks (CDs, DVDs, and Blu-rays) were from MPO Ibérica (Madrid, Spain).

2.2. Guided-mode resonance simulations

The response of the photonic crystals was simulated using the open-source EMUstack package (Björn Sturmberg, 2014; Dossou et al., 2012; Sturmberg et al., 2016). EMUstack implements a generalized scattering matrix method for calculating light propagation through multi-layered stacks of dispersive, lossy and nanostructured optical media.

The structure of the simulated guided-mode resonance grating was established according to the geometrical parameters of the internal structure of the compact disks, described in the bibliography (see Table S1). The calculated transmittance spectra were obtained by the set of transmission efficiency for each wavelength. During the simulation, the light source with a wavelength range of 400–800 nm was set as unpolarized, TM polarized or TE polarized; and the incident angle varied from 0° to 10°. The bioanalytical behavior of the guided-mode resonance grating was studied as a function of the thickness of the TiO2 layer, the thickness of the theoretical biolayer and the variation of surrounding media refractive index.

2.3. Fabrication

Raw polycarbonate plates containing the internal CD structure were obtained by peeling off all the other layers from a circular cut created in the outer edge of the disk, as described elsewhere.(Avella-Oliver et al., 2014) An analog strategy was employed to remove the protective polymeric layer (Durabis®) on the grooved relief of recordable Blu-ray disks. The internal DVD structure was obtained by disassembling both polycarbonate plates that compose these disks and keeping the one that contains the nanostructure (Avella-Oliver et al., 2017b). The remaining metallic layer on the disks was then removed by immersing them in a hydrochloric acid solution (1 M HCl) for 60 min at room temperature (RT). After that, they were rinsed with purified water and immersed in an ethanol bath for 1 min at RT in triplicate. Finally, they were rinsed with purified water and dried under air stream. In addition to these substrates, flat polycarbonate plates were also obtained from the bottom side of CD disks and used in this study as unstructured controls.

The CD, DVD and BD structured polycarbonate substrates and their unstructured counterpart were cut into squared chips of 1.5 × 1.2 cm using a drilling machine (Bungard CCD, Karo, Germany). The chips were then coated with several thicknesses of titanium dioxide at CIC nanoGUNE (Donostia, Gipuzkoa, Spain) using a UHV magnetron sputtering (ATC series, AJA International Inc., North Scituate, USA).

2.4. Characterization

The thickness of the deposited TiO_2 layers was characterized by X-Ray reflectivity/diffractometry using X'pert Pro (PANalytical, Almelo, The Netherlands), and surface topographies were analyzed by atomic force microscopy (AFM) measurements by nonconctact mode in air with a Multimode 8 microscope (Bruker, Billerica, USA). AFM averaged cross section profiles were obtained by averaging height values along the nanogroove direction.

2.5. Measurement setup

As described in Fig. 1A, the optical measurements were performed with a simple setup mainly constituted by a white light source (380–780 nm, ~ 15 W, Ace, Schott, Elmsford, USA) that hits the biosensing material and a fiber-coupled spectrometer that collects the transmitted light. A collimated light beam of 3 mm diameter was obtained by incorporating a plano-convex spherical lens (effective focal length of 150 mm) and an iris diaphragm. A custom 3D-printed holder was used for a reproducible alignment of the photonic crystals in the optical setup. Measurements were performed by averaging 50 scans (integration time of 1 s).

To characterize the photonic behavior of the materials, a linear

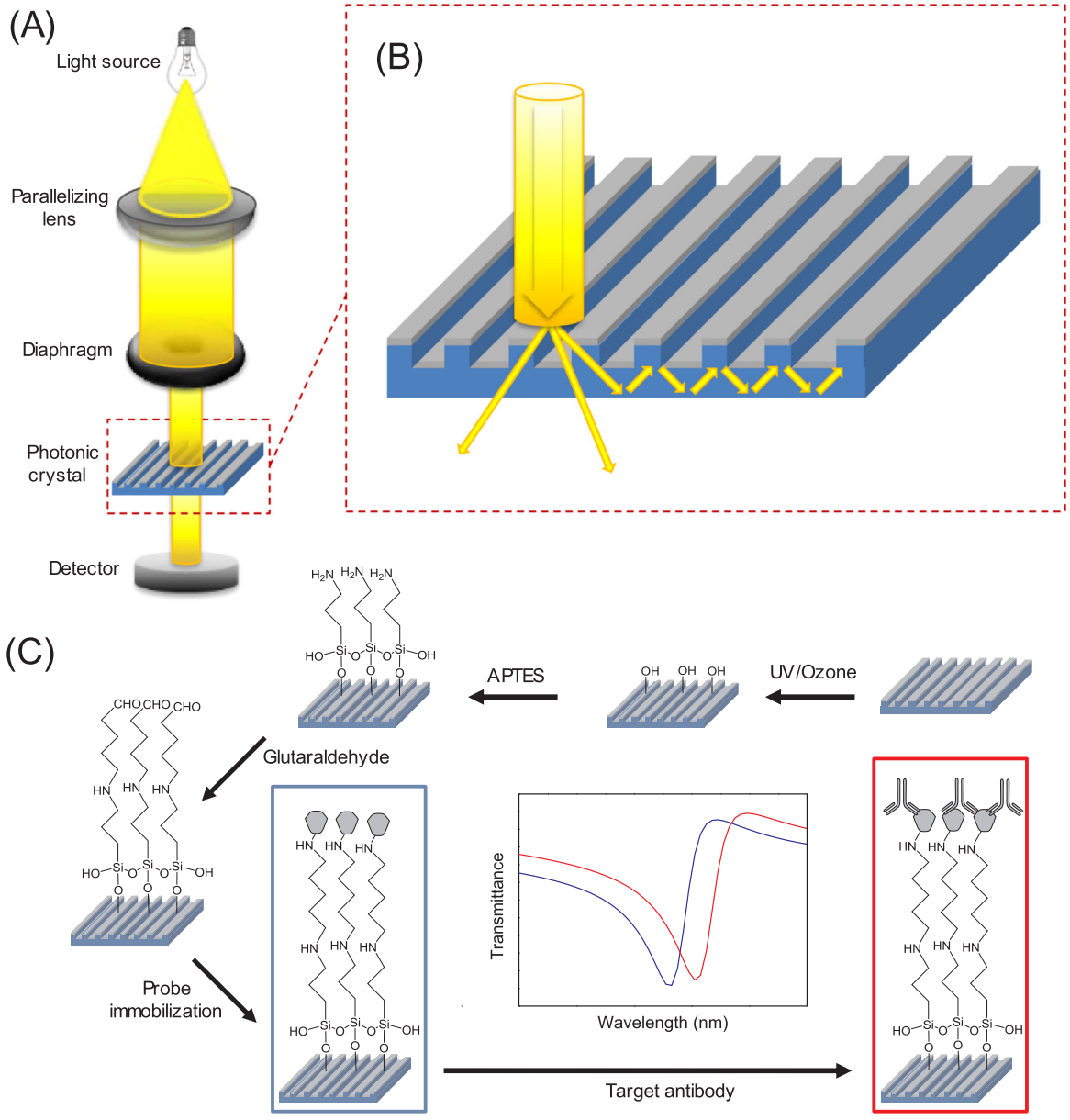

Fig. 1. (A) Scheme of the optical setup used in this work and the biosensing principle of linear photonic crystal slabs. (B) Illustration of the optical behavior of the linear photonic crystal slab. Some diffracted order by the grating is coupled into a guided mode and is guided through the waveguide. (C) Representation of the covalent probe immobilization and the target detection resulting in a wavelength shift of a resonance gap in the transmitted light.

setup configuration with a broad range visible spectrometer (AvaSpec-2048-USB2-RM, Avantes, Apeldoorn, The Netherlands) was used, together with a dedicated sample holder to screen the light incidence angles (Fig. S2A). A rotatable linear polarizer was placed between the diaphragm and the photonic crystal to assess the effect of the light polarization. Moreover, a custom PDMS flow cell (Fig. S3) was incorporated and connected to a peristaltic pump (Minipuls 2, Gilson, Middleton, USA) with a flow of 330 µL/min to inject solutions of different refractive index and to study their effects on the photonic crystal response. Each solution was injected for 10 min to make sure that the flow cell was completely full filled with the new dilution.

For the bioanalytical measurements, a mirror was included in the setup to analyze the photonic crystals in a horizontal position (Fig. S2B), thus enabling direct incubation of bioreagents in the system. Furthermore, a high resolution spectrophotometer (AvaSpec-2048TEC-USB2, Avantes, Apeldoorn, The Netherlands) with a wavelength range of 535–752 nm, was employed.

Measurements were performed by averaging 50 scans (integration time of 1 s). The resulting transmittance spectra were smoothed using a Savitzky-Golay filter (50 points window, second order). The position of the gaps was defined as the wavelength with minimal intensity, and it was determined using the Origin Pro 8 software (OriginLab Corporation, Northampton, USA).

2.6. Probe immobilization

The biochemical probes (BSA and IgGs) for the immunoassays studied in this work were covalently attached to the TiO_2 surface of the developed photonic crystals, as schematized in Fig. 1C. As described elsewhere (Gunda et al., 2014; Lou et al., 2017), the materials were first washed by immersion in EtOH for 5 min and then irradiated in a UV ozone cleaning system (UVOH 150 LAB, FHR, Ottendorf, Germany) for 10 min. After that, they were immersed in a 2% solution of (3-Aminopropyl)triethoxysilane in EtOH, incubated at RT for 30 min, rinsed with

EtOH, and dried in air stream. Subsequently, the chips were baked at 95 °C for 30 min, washed with PBS, and dried as before. Immediately after, the chips were immersed in a 2.5% (v/v) of glutaraldehyde in PBS, incubated at RT for 30 min, rinsed with deionized water, and dried by air stream. Lastly, the functionalized materials were immersed into probe solutions (100 μg mL^{-1} in PBS) for 30 min at RT, rinsed with PBS-T and deionized water, and dried as before.

2.7. Immunoassay

Biorecognition assays were performed by incubating target (rabbit anti-BSA IgG, CRP, or LDH) solutions in PBS-T on the probe-attached PC surfaces. Circular water repellent incubation areas (4 mm diameter) were delimited using a Mini PAP pen (Thermo Scientific, Madrid, Spain) and 40 μL of target solutions were dispensed and incubated at RT for 30 min, rinsed with PBS-T and deionized water, and dried in air stream. Dose-response curves were obtained by sequentially applying this protocol to solutions containing increasing target concentrations.

Wavelength shifts (Δλ) of the bandgaps in the transmission spectra were selected as analytical signal. Δλ values were calculated as the difference between the wavelength of a given bandgap before (immobilized probe) and after (incubated target) the assay. Averaged values and their standard deviations were obtained from six measurements of each sample. Noise was experimentally calculated as the standard deviation of ten blank replicates, signal-to-noise ratios were obtained by dividing Δλ by noise, and the limits of quantification and detection were inferred as the target concentrations whose SNR corresponds to 10 and 3, respectively.

3. Results and discussion

3.1. Guided-mode resonance performances

The bioanalytical capabilities of new photonic crystal slabs, based on different nanogrooved polycarbonate structures from standard recordable compact disks coated with TiO_2, were investigated. For this purpose, nanostructured patterns from CD, DVD, BD, and their unstructured counterpart, were coated with several TiO_2 thicknesses (0, 20, 40, 60, 80, and 100 nm). In all cases accurate coating values were obtained, as shown in Fig. S4. In this section, their GMR response is assessed by means of their simulated and experimental light filtering behavior and their simulated dose-response biorecognition curves.

First, it was observed that unstructured and CD substrates do not present photonic bands at any TiO_2 thickness (Fig. S5). As expected for the unstructured control, the absence of coupling grating disables the GMR activity. Regarding CD-based materials, the results indicate that coupling conditions are not met at these TiO_2 thicknesses in the visible range. This is also the case for thinner coatings on DVD (0–40 nm) and Blu-ray (0–20 nm) polycarbonate nanogrooved gratings, since they also display a flat transmission spectrum (Fig. S5 and Fig. 2).

More interestingly, the simulated and experimental results also show that the projected disk-based photonic crystal slabs are obtained by coating DVD and Blu-ray nanogrooved structures with thicker TiO_2 layers. DVD patterns coated with 60–100 nm (Fig. S5) and Blu-ray substrates coated by 40–100 nm (Fig. 2) present bandgaps in their experimental transmission spectra. These experimental observations are also in agreement with their calculated counterpart, where the systematic variations in the bandgaps position must come from experimental discrepancies. Moreover, these guided-mode resonances display a tunable behavior, and they move towards longer wavelengths when the coating thickness increases.

As observed in Fig. 2 and Fig. S5, the bandgaps measured by DVD-based substrates are wider and shallower than the ones presented by the developed Blu-ray photonic crystals. Since the projected transduction phenomena relies on bandgaps shifts, the proper determination of the bandgaps position (central wavelength) plays a key role in the performance of the resulting biosensor, and this determination is strongly hindered by wide and shallow bandgaps. Therefore, Blu-ray systems were selected, since their GMR activity display well-defined features in the transmission spectra.

The dose-response biorecognition curves developed onto the Blu-ray coated with TiO_2 were simulated. In the bibliography the refractive index of adsorbed protein layers is usually preset and its assumed value varies between 1.35 and 1.6 in ellipsometry and surface plasmon resonance calculations (Vörös, 2004). Assuming a refractive index of 1.47 (Skivesen et al., 2007) and a biolayer of 20 nm onto the surface, the analytical response of Blu-ray structures coated with different TiO_2 layer was calculated (Fig. S6). As the GMR-active Blu-ray gratings show similar analytical response, the criterion to choose a substrate was the definition (minimal width and maximal depth) of their experimental bandgaps, as explained above. In this sense, photonic crystals constituted by Blu-ray gratings coated with 80 nm of TiO_2 were selected in this study.

3.2. Topographic characterization

Once these Blu-ray photonic crystals were chosen, their structural features were characterized. Blu-ray disks have a spiral-shaped internal grooved structure that towards the edges of the disks is well approximated by lineal gratings. This structure works perfectly as digital data storage, but its physical fabrication is not totally flawless. Fig. S7 shows the surface topography of this structure before and after being coated with the TiO_2 layer by AFM. As can be appreciated, the grating is slightly irregular, presenting zones were the bottom of the grove is wider than others and vice versa. Moreover, the grating has a nearly rectangular profile, but the wall of the grating is not perfectly vertical. These facts affect the GMR activity, and can produce irrelevant differences between the experimental and calculated transmission spectra, like peak width and position.

On the other hand, the TiO_2 coating did not modify the profile of the grating but it can be appreciated that the TiO_2 layer had a granulated topography. As can be observed in Fig. S8, the unstructured substrate shown a slightly rough wavy surface (RMS of 0.24 ± 0.03 nm), however when it was coated with a TiO_2 layer, the ripples of the surface were filled and it became much rougher (RMS of 0.69 ± 0.06 nm). Therefore, the TiO_2 coating kept the period, depth and shape of the nanogrooved structure constant but it increased its roughness.

3.3. Photonic response

As shown above, the selected photonic crystal interacts with incident light to provide defined bandgaps in the transmission spectrum. The relative configuration of the incident light versus the features of the nanostructured pattern plays a key role in the GMR response. This section explores this issue in order to understand it and fully exploit the biosensing capabilities of these photonic crystal slabs. First, we studied the effect of the relative orientation between the light polarization and the grooved nanostructure. As shown in Fig. 2, the developed materials generate two different transmission bandgaps upon unpolarized light irradiation, in concordance with the GMR activity of these type of materials (Moghaddas et al., 2014).

We have experimentally observed that the relative intensity of these bandgaps can be modulated by means of polarization of the incident light. As shown in Fig. 3A, linearly polarized light oriented in the nanogroove direction (0°) only generates the longer wavelength gap. The intensity of this gap gradually decreases when the polarization angle increases, whereas the shorter wavelength gap displays the opposite trend. Irradiating light perpendicularly polarized to the nanogroove (90°) uniquely displays the gap centered at 525 nm. Considering the simulations (Fig. S9A), the 525 nm and the 590 nm gaps come from the coupling of the diffracted transverse magnetic (TM) and transverse electric (TE) polarization, respectively. From these results along with

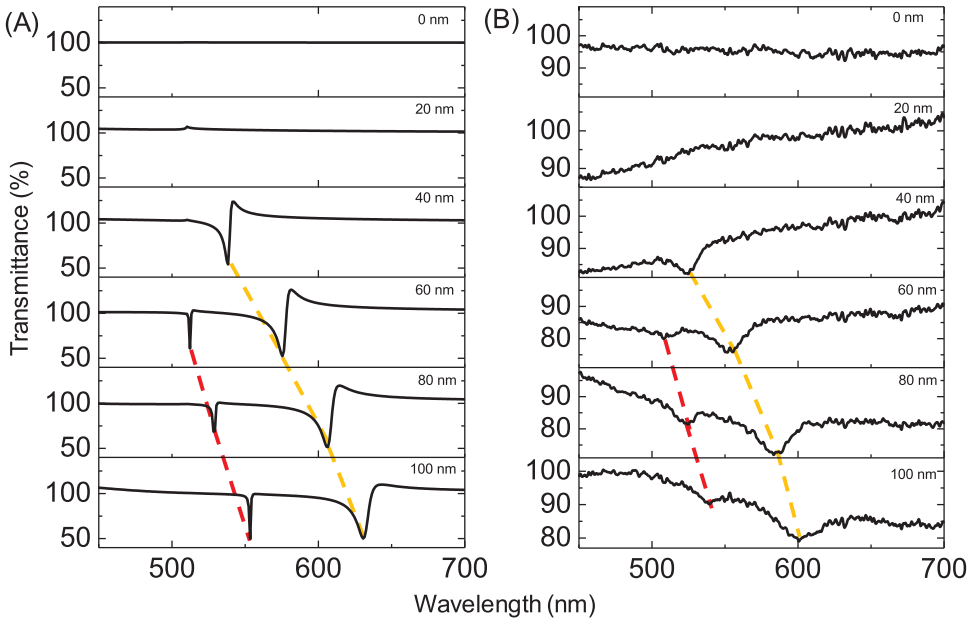

Fig. 2. (A) Simulated and (B) experimental transmission spectra of the GMR-active materials based on Blu-ray nanogrooved patterns coated with TiO_2, where dashed lines indicate the trend of the wavelength shift.

those in Section 3.1, perpendicular polarization was selected to filter out TM bands, thus isolating TE gaps to be used for biosensing.

We also studied the effect of the light incidence angle on the GMR response of these photonic crystal slabs. As experimentally observed (Fig. S10B), modifying this parameter along the parallel direction of the nanogroove does not display any influence on the transmission spectra. This is in agreement with the calculated data as can be observed in Fig. S10A. However, non-orthogonal light incidence angles along the perpendicular direction of the nanogrooves split the gaps into two different bands. As shown in Fig. 3B, the width of this splitting increases together with the incidence angle, whereas the averaged wavelength of both gaps remains constant. This characteristic, which is proper of this type of substrates, is in agreement with the simulated transmittance spectra and is also displayed by the TE gaps (Fig. S9B) (Wang and Magnusson, 1993).

On the one hand, this splitting represents a straightforward and versatile strategy namely to tune the photonic response of these materials to the desired wavelength range employed in a biosensing setup. On the other hand, we also exploited this phenomenon to improve the quality of the bioanalytical results obtained with these photonic crystals. As observed in Fig. 3B, tiny angle modifications generate significant splits, and this great sensitivity on the irradiation angle constitutes an important potential imprecision source for experimental measurements based on the $\Delta\lambda$ of a single peak. As an alternative, we employed a custom holder tilted 5° in the perpendicular direction of the nanogrooves, and used the averaged wavelength of both gaps as the analytical signal. Given the symmetry of the gaps splitting, this strategy provides measurements more insensitive to the incidence angle, thus enabling more robust bioanalytical measurements.

Regarding inter-chip precision, we have experimentally determined

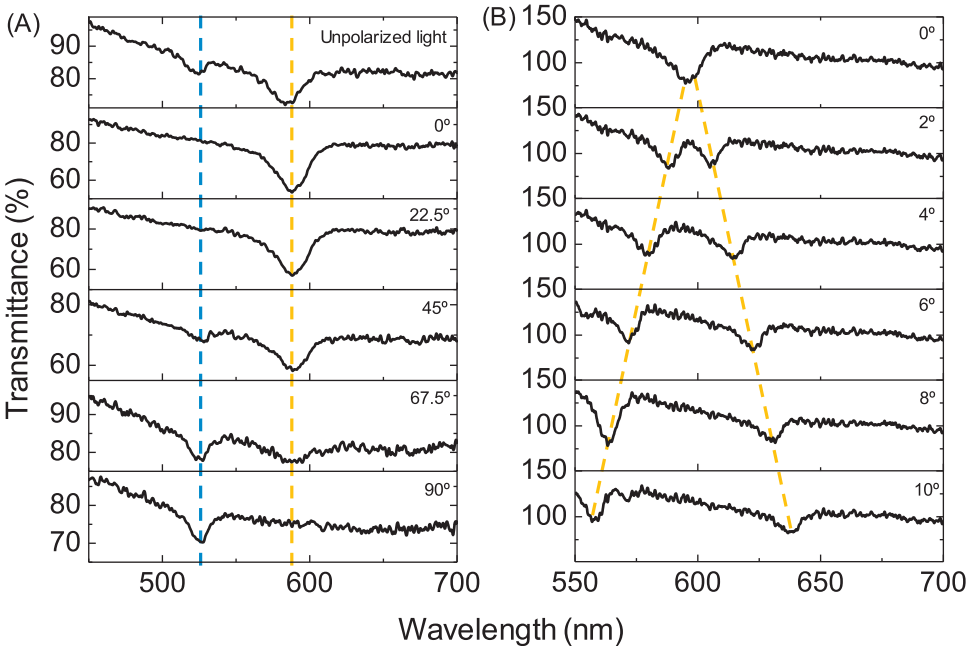

Fig. 3. Experimental transmittance spectra upon (A) different linear polarization orientations where the 0° angle means that the polarized light is orientated perpendicular to the nanogroove direction and (B) a range of light incidence angles along the perpendicular nanogroove direction. The width of this splitting increases together with the incidence angle, whereas the averaged wavelength of both gaps remains constant. The blue and yellow dashed lines help to follow the GMR positions of the TM and TE modes, respectively.

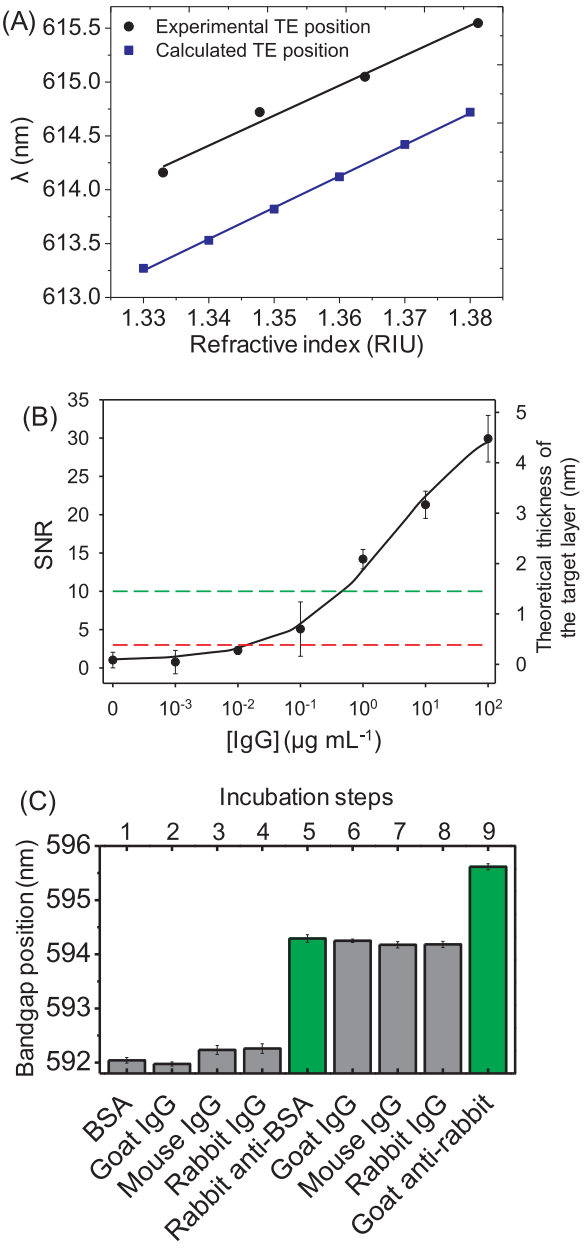

Fig. 4. (A) Calculated (blue square) and experimental (black dot) refractometic response in bulk solutions on the photonic crystal. A linear fit is given for both: calculated (R^2 = 0.9993) and experimental (R^2 =0.9813) with a sensitivity of 29.2 ± 0.4 and 28 ± 2 nm RIU^{-1}, respectively. (B) Dose-response curve using the Blu-ray coated with 80 nm of TiO_2 for IgG analysis. Experimental data fitted to four-parameter logistic equation and correlated with the theoretical thickness of the target layer. The green and red dashed lines mark the SNR thresholds for quantification and detection limits, respectively. (C) Photonic crystal biosensor selectivity assay. The bandgap position corresponds to the GMR wavelength after each consecutive incubation of several target antibodies, where averaged values and standard deviations were calculated from 6 replicated measurements.

a standard deviation of the bandgap position of 0.2 nm (considering 6 different chips). This non-negligible value must come from heterogeneities on the TiO_2 coatings in different chips, and it may hinder the bioanalytical determinations. To minimize this issue with the proof-of-concept detection system arranged in this development, the custom sample holder was also used to fix the position of the chip along the different stages of the subsequent experimental immunoassays.

3.4. Immunosensing

Once characterized the photonic crystals and stablished a detection procedure, we explore the performance of these materials in experimental bioanalytical systems. For that, the first approximation was to characterize their refractometric response by measuring the bandgap shifts generated by bulk solutions on their surface. Sucrose solutions with refractive indexes from 1.33 to 1.38 were placed on the photonic crystal and its GMR response was analyzed. As observed in Fig. 4A, these measurements displayed a well-correlated (R^2 = 0.9813) linear dependence between the refractive index and the bandgap Δλ. An experimental refractometric sensitivity of 28 ± 2 nm RIU^{-1} was obtained from the slope of the fitting, which is in the range of the state-of-the-art photonic crystal slabs developments (Hermannsson et al., 2015; Nazirizadeh et al., 2010; Sørensen et al., 2018). These results are in agreement with the simulated data, which bandgap positions and theoretical sensitivity (29.2 ± 0.4 nm RIU^{-1}) are very similar.

To demonstrate the bioanalytical performance of these photonic crystal slabs, herein we first employed a model immunoassay based on BSA as probes and anti-BSA IgGs as targets. This is a representative, well-known, and practical immunoassay typically used as a model system for proof-of-concept purposes (Yin et al., 2005). Also, given the key role of albumins in multitude of biological functions (Avella-Oliver et al., 2017a), the results with this system may provide insights into prospective applications. On the other hand, BSA is one of the main allergens present in cow's milk and beef (de Silva et al., 2017). Furthermore, BSA may be responsible for the autoimmune response leading to diabetes mellitus in people genetically susceptible to this disease (Kooser et al., 2003).

According to our simulations (Fig. S11), the system is more sensitive to biorecognition events when they are in air rather than in aqueous solutions. A theoretical biolayer of 10 nm thickness generates double and almost triple the wavelength shift if the media is air instead of water, for the TM and TE respectively. This happens because the refractive index of the biological molecules is more similar to water than air and therefore, there are more refractive index changes when the biological event is measured dry. Thus, the assays were performed by sequential incubations into the detection setup and analyzed by end-point measurements after IgG incubations.

As shown Fig. 4B, a well-correlated dose-response sigmoidal curve (R^2 = 0.993) was obtained in this label-free assay for IgGs determination. A quantification limit of 465 ng mL^{-1} (3.1 nM) and a detection limit of 16 ng mL^{-1} (100 pM) of IgG are inferred from this curve, which is in the sensitivity range of other similar materials fabricated by nanoimprinting lithography (Inan et al., 2017; Jahns et al., 2015), as well as in other new label-free optical biosensing developments (Chen et al., 2018; Hao et al., 2018; Shi et al., 2018). In particular, it improves about one order of magnitude the detection limit achieved in another recent development with this same immunological system using diffractive protein gratings (Avella-Oliver et al., 2017a).

The right axis in Fig. 4B indicates the estimated thicknesses of the biological layer on the photonic crystal along the biorecognition curve. For that, the calculated thickness (Fig. S12) corresponding to each experimental wavelength shift was determined and plotted in the graph. Since antibodies can bind their targets in several orientations, this approach must be understood as an averaged thickness (Tan et al., 2008; Trilling et al., 2013). As shown in Fig. 4B, the wavelength shift of the highest target concentration in the curve displays an estimated biolayer thickness of about 4 nm. This can be attributed to an ideal scenario where an homogeneous layer of antibodies lie on the surface in flat-on orientation, or an arrangement of different orientations and uncoated areas with an averaged thickness of 4 nm.

To evaluate the selectivity of this biosensor, the response of the system upon consecutive incubations of high concentrations (100 μg mL^{-1}) of specific and non-specific IgGs was studied. As observed in Fig. 4C, after immobilizing probe BSA on the photonic crystal

(step 1), the subsequent incubations of non-specific IgGs (steps 2, 3, and 4) generated minor wavelength shifts from the bandgap position. This fact indicates that these incubations involve rather small increases of the biolayer thickness, which points out a minor interaction of these bioreagents. Then, rabbit anti-BSA specifically interacted with the immobilized probe as expected (step 5), and this biorecognition event generated a substantial displacement of the bandgap. After that, non-specific IgGs were also consecutively incubated as before (steps 6, 7, and 8), leading to negligible responses in all the cases. These results point out the selectivity of the proposed approach, as well as a minor non-specific binding obtained in this assay conditions, even without using specific blocking or backfilling stages.

On the other hand, Fig. 4C also shows that the incubation of goat anti-rabbit after the assay (step 9) generates an important bandgap displacement (about 1.5 nm), which indicates the specific recognition of the bound rabbit anti-BSA by this secondary antibody. This approach is frequently employed as a signal amplification strategy to increase the sensitivity in biorecognition assays. For example, similar signal enhancements to the one obtained in this study (about 1.5-fold) have also been reported using secondary antibodies in other label-free developments based on ring and disk resonators, and Bragg gratings (Schmidt et al., 2014). In addition to suggest a potential strategy to increase sensitivity, these results also prove the performance of the system in more complex schemes involving sequential biorecognition events.

To provide insights into the performance of the developed biosensing materials beyond the model BSA/anti-BSA system, the response of these materials in two different immunoassays to the biomarkers CRP and LDH, was also studied. In both cases, specific antibody probes were immobilized on the photonic crystals to recognize these target proteins. Regarding CRP, a well correlated wavelength shift along target concentrations was obtained in the corresponding dose-response curve (R^2 = 0.996), as observed in Fig. 5A. From this curve, a quantification limit of 7 μg mL^{-1} (304 nM) and a detection limit of 2 μg mL^{-1} (87 nM) are inferred for this immunoassay. These sensitivities are much lower than the ones obtained in the other systems addressed in this study, which points out the lower binding affinities of the probes used in this immunoassay. However, despite these low SNR values, this sensitivity is in the concentration range of CRP in healthy humans plasma (between 3 and 10 μg mL^{-1}), which increases dramatically under cardiovascular diseases, inflammations, and infections (Kowalczyk et al., 2018; Uddin et al., 2018).

On the other hand, LDH is an enzyme present in human tissues. Its concentration in blood is low for healthy humans, whereas high levels of LDH indicates tissue damage processes. Monitoring its concentration is for example commonly used during the treatment of brain and bladder cancers (Cacho-Díaz et al., 2018; Chuang et al., 2015), and it is also useful for physicians and coaches to design appropriate trainings (Brancaccio et al., 2008). As observed in the Fig. 5B, this immunoassay displays a well-correlated dose-response curve (R^2 = 0.996), reaching a quantification limit of 50 ng mL^{-1} (36 nM) and a detection limit of 18 ng mL^{-1} (13 nM). The concentration of LDH is typically determined from its enzymatic activity (Kaja et al., 2017) and quantified as international units per liter (U L^{-1}). Considering the activity of the LDH used (709 U mg^{-1}), the reported quantification and detection limits in this study become 35.6 U L^{-1} and12.8 U L^{-1}, respectively. This sensitivity is in the lineal range provided by commercial assay kits for LDH (1–100 U L^{-1}),[1,2] whereas the developed approach enables a direct analysis without the needed of enzymatic reactions.

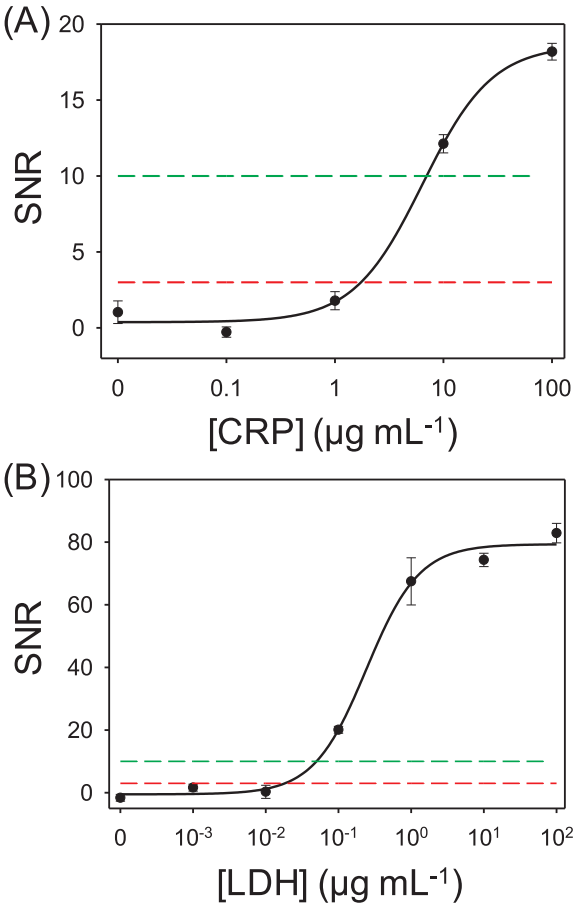

Fig. 5. Dose-response curves using the Blu-ray coated with 80 nm of TiO_2 for (A) CRP and (B) LDH immunoassays. Experimental data fitted to four-parameter logistic equation. The green and red dashed lines mark the SNR thresholds for quantification and detection limits, respectively.

4. Conclusions

In this study, we have developed simple and large-scale photonic crystal slabs for label-free biosensing, based on the grooved structure of recordable compact disks coated with TiO_2. Both experimental and simulated results have demonstrated the GMR activity of these materials, which can be easily tuned by modifying the TiO_2 thickness and the angle of the incidence light. Blu-ray nanogrooves coated by 80 nm of TiO_2 display well-defined bandgaps, whose displacement reports a refractometric sensitivity of 28 nm RIU^{-1}. More importantly, these bandgap shifts enable to transduce unlabeled biorecognition events in a selective fashion, as demonstrated in an immunochemical model assay to quantify IgGs as well as to determine the biomarkers C-reactive protein and lactate dehydrogenase (detection limits of 0.1, 87, and 13 nM, respectively). As a limitation, more homogenous depositions of TiO_2 layers would reduce the inter-chip precision and favor the impact of these materials in practical applications. Besides, it is worth to highlight that the tunability, simplicity, low cost, and scalability of these photonic crystals provides them with appealing features for prospective studies towards label-free point-of-care developments. Along these lines, regular disk drives could potentially be adapted to become simple and robust analyzers for these disk-based photonic crystals. Finally, this study also suggests future investigations to explore the potential of these nanomaterials to transduce binding events coming from biorecognition assays of different natures.

Notes

The authors declare no competing financial interest.

[1] ab102526 from Abcam.
[2] Mak066 from Merck.

Acknowledgment

This research was supported by FEDER grants and the Spanish Ministry of Economy and Competitiveness projects (CTQ2013-45875-R and CTQ2016-75749-R).

Appendix A. Supplementary material

Supplementary data associated with this article can be found in the online version at doi:10.1016/j.bios.2018.11.005.

References

Avella-Oliver, M., Morais, S., Carrascosa, J., Puchades, R., Maquieira, Á., 2014. Total analysis systems with thermochromic etching discs technology. Anal. Chem. 86, 12037–12046. https://doi.org/10.1021/ac502640j.

Avella-Oliver, M., Morais, S., Puchades, R., Maquieira, Á., 2016. Towards photochromic and thermochromic biosensing. Trends Anal. Chem. https://doi.org/10.1016/j.trac.2015.11.021.

Avella-Oliver, M., Carrascosa, J., Puchades, R., Maquieira, Á., 2017a. Diffractive protein gratings as optically active transducers for high-throughput label-free immunosensing. Anal. Chem. 89, 9002–9008. https://doi.org/10.1021/acs.analchem.7b01649.

Avella-Oliver, M., Puchades, R., Wachsmann-Hogiu, S., Maquieira, A., 2017b. Label-free SERS analysis of proteins and exosomes with large-scale substrates from recordable compact disks. Sens. Actuators B 252, 657–662. https://doi.org/10.1016/j.snb.2017.06.058.

Brancaccio, P., Maffulli, N., Buonauro, R., Limongelli, F.M., 2008. Serum enzyme monitoring in sports medicine. Clin. Sports Med. 27, 1–18. https://doi.org/10.1016/J.CSM.2007.09.005.

Cacho-Díaz, B., Lorenzana-Mendoza, N.A., Reyes-Soto, G., Hernández-Estrada, A., Monroy-Sosa, A., Guraieb-Chahin, P., Cantu-de-León, D., 2018. Lactate dehydrogenase as a prognostic marker in neoplastic meningitis. J. Clin. Neurosci. 51, 39–42. https://doi.org/10.1016/j.jocn.2018.02.014.

Carrascosa, L.G., Huertas, C.S., Lechuga, L.M., 2016. Prospects of optical biosensors for emerging label-free RNA analysis. Trends Anal. Chem. 80, 177–189. https://doi.org/10.1016/j.trac.2016.02.018.

Chen, W.T., Li, S.S., Chu, J.P., Feng, K.C., Chen, J.K., 2018. Fabrication of ordered metallic glass nanotube arrays for label-free biosensing with diffractive reflectance. Biosens. Bioelectron. 102, 129–135. https://doi.org/10.1016/j.bios.2017.10.023.

Chuang, C.-H., Wu, T.-F., Chen, C.-H., Chang, K.-C., Ju, J.-W., Huang, Y.-W., Van Nhan, V., 2015. Lab on a chip for multiplexed immunoassays to detect bladder cancer using multifunctional dielectrophoretic manipulations. Lab Chip 15, 3056–3064. https://doi.org/10.1039/C5LC00352K.

Citartan, M., Gopinath, S.C.B., Tominaga, J., Tang, T.-H., Deng, W., Joo, S.W., Park, Q.H., Ihee, H., Kim, B., 2013. Label-free methods of reporting biomolecular interactions by optical biosensors. Analyst 138, 3576–3592. https://doi.org/10.1039/c3an36828a.

Dossou, K.B., Botten, L.C., Asatryan, A.A., Sturmberg, B.C.P., Byrne, M.A., Poulton, C.G., McPhedran, R.C., de Sterke, C.M., 2012. Modal formulation for diffraction by absorbing photonic crystal slabs. J. Opt. Soc. Am. A 29, 817. https://doi.org/10.1364/JOSAA.29.000817.

Fathi, F., Rahbarghazi, R., Rashidi, M.R., 2018. Label-free biosensors in the field of stem cell biology. Biosens. Bioelectron. https://doi.org/10.1016/j.bios.2017.10.028.

Fenzl, C., Hirsch, T., Wolfbeis, O.S., 2014. Photonic crystals for chemical sensing and biosensing. Angew. Chem. - Int. Ed. https://doi.org/10.1002/anie.201307828.

Gunda, N.S.K., Singh, M., Norman, L., Kaur, K., Mitra, S.K., 2014. Optimization and characterization of biomolecule immobilization on silicon substrates using (3-aminopropyl)triethoxysilane (APTES) and glutaraldehyde linker. Appl. Surf. Sci. 305, 522–530. https://doi.org/10.1016/j.apsusc.2014.03.130.

Hao, D., Hu, C., Grant, J., Glidle, A., Cumming, D.R.S., 2018. Hybrid localized surface plasmon resonance and quartz crystal microbalance sensor for label free biosensing. Biosens. Bioelectron. 100, 23–27. https://doi.org/10.1016/j.bios.2017.08.038.

Hermannsson, P.G., Sørensen, K.T., Vannahme, C., Smith, C.L.C., Klein, J.J., Russew, M.-M., Grützner, G., Kristensen, A., 2015. All-polymer photonic crystal slab sensor. Opt. Express 23, 16529–16539. https://doi.org/10.1364/OE.23.016529.

Inan, H., Poyraz, M., Inci, F., Lifson, M.A., Baday, M., Cunningham, B.T., Demerci, U., 2017. Photonic crystals: emerging biosensors and their promise for point-of-care applications. Chem. Soc. Rev. 366, 366–388. https://doi.org/10.1039/c6cs00206d.

Jahns, S., Bräu, M., Meyer, B.-O., Karrock, T., Gutekunst, S.B., Blohm, L., Selhuber-Unkel, C., Buhmann, R., Nazirizadeh, Y., Gerken, M., 2015. Handheld imaging photonic crystal biosensor for multiplexed, label-free protein detection. Biomed. Opt. Express 6, 3724–3736. https://doi.org/10.1364/BOE.6.003724.

Joannopoulos, J.J.D., Johnson, S., Winn, J.N.J., Meade, R.R.D., 2008. Photonic crystals: molding the flow of light, second. ed, Time. New Jersey.

Kaja, S., Payne, A.J., Naumchuk, Y., Koulen, P., 2017. Quantification of lactate dehydrogenase for cell viability testing using cell lines and primary cultured astrocytes. Curr. Protoc. Toxicol. 72, 2.26.1–2.26.10. https://doi.org/10.1002/cptx.21.

Karrock, T., Paulsen, M., Gerken, M., 2017. Flexible photonic crystal membranes with nanoparticle high refractive index nanoparticle layers. Beilstein J. Nanotechnol. 8, 203–209. https://doi.org/10.3762/bjnano.8.22.

Kettler, H., White, K., Hawkes, S., 2004. Mapping the landscape of diagnostics for sexually transmitted infections: Key findings and recommandations. Unicef/Undp/World Bank/Who 1–44. doi:WHO reference number: TDR/STI/IDE/04.1.

Konopsky, V.N., Alieva, E.V., 2007. Photonic crystal surface waves for optical biosensors. Anal. Chem. 79, 4729–4735. https://doi.org/10.1021/ac070275y.

Kooser, A., Manygoats, K., Eastman, M.P., Porter, T.L., 2003. Investigation of the antigen antibody reaction between anti-bovine serum albumin (a-BSA) and bovine serum albumin (BSA) using piezoresistive microcantilever based sensors. Biosens. Bioelectron. 19, 503–508. https://doi.org/10.1016/S0956-5663(03)00221-5.

Kowalczyk, A., Sęk, J.P., Kasprzak, A., Poplawska, M., Grudzinski, I.P., Nowicka, A.M., 2018. Occlusion phenomenon of redox probe by protein as a way of voltammetric detection of non-electroactive C-reactive protein. Biosens. Bioelectron. 117, 232–239. https://doi.org/10.1016/j.bios.2018.06.019.

Li, Z., Li, F., Xing, Y., Liu, Z., You, M., Li, Y., Wen, T., Qu, Z., Ling, Li, X., Xu, F., 2017. Pen-on-paper strategy for point-of-care testing: rapid prototyping of fully written microfluidic biosensor. Biosens. Bioelectron. 98, 478–485. https://doi.org/10.1016/j.bios.2017.06.061.

Lin, H.A., Huang, C.S., 2016. Linear variable filter based on a gradient grating period Guided-Mode Resonance filter. IEEE Photonics Technol. Lett. 28, 1042–1045. https://doi.org/10.1109/LPT.2016.2524655.

Lin, Y.-C., Hsieh, W.-H., Chau, L.-K., Chang, G.-E., 2017. Intensity-detection-based guided-mode-resonance optofluidic biosensing system for rapid, low-cost, label-free detection. Sens. Actuators B 250, 659–666. https://doi.org/10.1016/j.snb.2017.04.187.

López-Muñoz, G.A., Estevez, M.-C.C., Peláez-Gutierrez, E.C., Homs-Corbera, A., García-Hernandez, M.C., Imbaud, J.I., Lechuga, L.M., 2017. A label-free nanostructured plasmonic biosensor based on Blu-ray discs with integrated microfluidics for sensitive biodetection. Biosens. Bioelectron. 96, 260–267. https://doi.org/10.1016/j.bios.2017.05.020.

Lou, X., Zhu, A., Luo, Q., Zhang, Y., Long, F., Klibanov, M.A., Long, F., 2017. Effects of organic solvents on immunosensing assays for small molecules based on an optofluidic immunosensing platform. Anal. Methods 9, 5731–5740. https://doi.org/10.1039/C6AY03373C.

Michael, I., Kim, T.-H., Sunkara, V., Cho, Y.-K., 2016. Challenges and opportunities of centrifugal microfluidics for extreme Point-of-Care Testing. Micromachines 7, 32. https://doi.org/10.3390/mi7020032.

Moghaddas, S.A.J., Shahabadi, M., Mohammad-Taheri, M., 2014. Guided mode resonance sensor with enhanced surface sensitivity using coupled cross-stacked gratings. IEEE Sens. J. 14, 1216–1222. https://doi.org/10.1109/JSEN.2013.2294536.

Morais, S., Puchades, R., Maquieira, Á., 2016. Disc-based microarrays: principles and analytical applications. Anal. Bioanal. Chem. 408, 4523–4534. https://doi.org/10.1007/s00216-016-9423-1.

Nazirizadeh, Y., Bog, U., Sekula, S., Mappes, T., Lemmer, U., Gerken, M., 2010. Low-cost label-free biosensors using photonic crystals embedded between crossed polarizers. Opt. Express 18, 19120–19128. https://doi.org/10.1364/OE.18.019120.

Nikov, R.G., Dikovska, A.O., Nedyalkov, N.N., Avdeev, G.V., Atanasov, P.A., 2017. Au nanostructure fabrication by pulsed laser deposition in open air: influence of the deposition geometry. Beilstein J. Nanotechnol. 8, 2438–2445. https://doi.org/10.3762/bjnano.8.242.

Ranjan, R., Esimbekova, E.N., Kratasyuk, V.A., 2017. Rapid biosensing tools for cancer biomarkers. Biosens. Bioelectron. 87, 918–930. https://doi.org/10.1016/j.bios.2016.09.061.

Schmidt, S., Flueckiger, J., Wu, W., Grist, S.M., Talebi Fard, S., Donzella, V., Khumwan, P., Thompson, E.R., Wang, Q., Kulik, P., Wang, X., Sherwali, A., Kirk, J., Cheung, K.C., Chrostowski, L., Ratner, D., 2014. Improving the performance of silicon photonic rings, disks, and Bragg gratings for use in label-free biosensing. In: Mohseni, H., Agahi, M.H., Razeghi, M. (Eds.), International Society for Optics and Photonics, pp. 91660M. https://doi.org/10.1117/12.2062389.

Shafiee, H., Lidstone, E.A., Jahangir, M., Inci, F., Hanhauser, E., Henrich, T.J., Kuritzkes, D.R., Cunningham, B.T., Demirci, U., 2014. Nanostructured optical photonic crystal biosensor for HIV viral load measurement. Sci. Rep. 4, 1–7. https://doi.org/10.1038/srep04116.

Shi, Y., Zhang, Q., Zhai, T.-T., Zhou, Y., Yang, D.-R., Wang, F.-B., Xia, X.-H., 2018. Localized surface plasmon resonance enhanced label-free photoelectrochemical immunoassay by Au-MoS2 nanohybrid. Electrochim. Acta 271, 361–369. https://doi.org/10.1016/j.electacta.2018.03.167.

de Silva, R., Dasanayake, W.M.D.K., Wickramasinhe, G.D., Karunatilake, C., Weerasinghe, N., Gunasekera, P., Malavige, G.N., 2017. Sensitization to bovine serum albumin as a possible cause of allergic reactions to vaccines. Vaccine 35, 1494–1500. https://doi.org/10.1016/j.vaccine.2017.02.009.

Skivesen, N., Têtu, A., Kristensen, M., Kjems, J., Frandsen, L.H., Borel, P.I., 2007. Photonic-crystal waveguide biosensor. Opt. Express 15, 3169–3176. https://doi.org/10.1364/OE.15.003169.

Sørensen, K.T., Ingvorsen, C.B., Nielsen, L.H., Kristensen, A., 2018. Effects of water-absorption and thermal drift on a polymeric photonic crystal slab sensor. Opt. Express 26, 5416–5422. https://doi.org/10.1364/OE.26.005416.

St John, A., Price, C.P., 2014. Existing and emerging technologies for point-of-care testing. Clin. Biochem Rev. 353, 155–167.

Sturmberg, B.C.P., Dossou, K.B., Lawrence, F.J., Poulton, C.G., McPhedran, R.C., Martijn De Sterke, C., Botten, L.C., 2016. EMUstack: an open source route to insightful electromagnetic computation via the Bloch mode scattering matrix method. Comput. Phys. Commun. 202, 276–286. https://doi.org/10.1016/j.cpc.2015.12.022.

Sturmberg, Björn, 2014. EMUstack [WWW Document]. URL ⟨http://www.physics.usyd.edu.au/emustack/index.html⟩ (Accessed 23 October 2018).

Su, H., Cheng, X.R., Endo, T., Kerman, K., 2018. Photonic crystals on copolymer film for label-free detection of DNA hybridization. Biosens. Bioelectron. 103, 158–162. https://doi.org/10.1016/j.bios.2017.12.013.

Tan, Y.H., Liu, M., Nolting, B., Go, J.G., Gervay-Hague, J., Liu, G.Y., 2008. A nanoengineering approach for investigation and regulation of protein immobilization. ACS

Nano 2, 2374–2384. https://doi.org/10.1021/nn800508f.
Threm, D., Nazirizadeh, Y., Gerken, M., 2012. Photonic crystal biosensors towards on-chip integration. J. Biophotonics 5, 601–616. https://doi.org/10.1002/jbio.201200039.
Trilling, A.K., Beekwilder, J., Zuilhof, H., 2013. Antibody orientation on biosensor surfaces: a minireview. Analyst 138, 1619–1627. https://doi.org/10.1039/c2an36787d.
Uddin, R., Donolato, M., Hwu, E.-T., Hansen, M.F., Boisen, A., 2018. Combined detection of C-reactive protein and PBMC quantification from whole blood in an integrated lab-on-a-disc microfluidic platform. Sens. Actuators B 272, 634–642. https://doi.org/10.1016/j.snb.2018.07.015.
Vashist, S.K., Luppa, P.B., Yeo, L.Y., Ozcan, A., Luong, J.H.T., 2015. Emerging technologies for next-generation point-of-care testing. Trends Biotechnol. https://doi.org/10.1016/j.tibtech.2015.09.001.
Vörös, J., 2004. The density and refractive index of adsorbing protein layers. Biophys. J. 87, 553–561. https://doi.org/10.1529/biophysj.103.030072.
Wang, S.S., Magnusson, R., 1993. Theory and applications of guided-mode resonance filters. Appl. Opt. 32, 2606. https://doi.org/10.1364/AO.32.002606.
Wang, Y., Ali, M.A., Chow, E.K.C., Dong, L., Lu, M., 2018. An optofluidic metasurface for lateral flow-through detection of breast cancer biomarker. Biosens. Bioelectron. 107, 224–229. https://doi.org/10.1016/j.bios.2018.02.038.
Yamada, Y., Ito, K., Miura, A., Iizuka, H., Wakayama, H., 2017. Simple and scalable preparation of master mold for nanoimprint lithography. Nanotechnology 28. https://doi.org/10.1088/1361-6528/aa6a9f.
Yan, H., Yang, C.-J., Tang, N., Zou, Y., Chakravarty, S., Roth, A., Chen, R.T., 2017. Specific detection of antibiotics by silicon-on-chip photonic crystal biosensor arrays. IEEE Sens. J. 17, 5915–5919. https://doi.org/10.1109/JSEN.2017.2734885.
Yin, X.B., Qi, B., Sun, X., Yang, X., Wang, E., 2005. 4-(Dimethylamino)butyric acid labeling for electrochemiluminescence detection of biological substances by increasing sensitivity with gold nanoparticle amplification. Anal. Chem. 77, 3525–3530. https://doi.org/10.1021/ac0503198.
Yu, H.Z., Li, Y., Ou, L.M.L., 2013. Reading disc-based bioassays with standard computer drives. Acc. Chem. Res. 46, 258–268. https://doi.org/10.1021/ar300104b.
Zanchetta, G., Lanfranco, R., Giavazzi, F., Bellini, T., Buscaglia, M., 2017. Emerging applications of label-free optical biosensors. Nanophotonics 6, 627–645. https://doi.org/10.1515/nanoph-2016-0158.
Zhang, J., Yang, J., Lu, H., Wu, W., Huang, J., Chang, S., 2015. Subwavelength TE/TM grating coupler based on silicon-on-insulator. Infrared Phys. Technol. 71, 542–546. https://doi.org/10.1016/j.infrared.2015.06.018.
Zlatanovic, S., Mirkarimi, L.W., Sigalas, M.M., Bynum, M.A., Chow, E., Robotti, K.M., Burr, G.W., Esener, S., Grot, A., 2009. Photonic crystal microcavity sensor for ultracompact monitoring of reaction kinetics and protein concentration. Sens. Actuators B 141, 13–19. https://doi.org/10.1016/j.snb.2009.06.007.